The Crystal Structure of Citrate Synthase from the Hyperthermophilic Archaeon *Pyrococcus furiosus* at 1.9 Å Resolution[†,‡]

Rupert J. M. Russell, Jacqueline M. C. Ferguson, David W. Hough, Michael J. Danson, and Garry L. Taylor*

School of Biology and Biochemistry, University of Bath, Bath BA2 7AY, U.K.

Received March 7, 1997; Revised Manuscript Received May 12, 1997[⊗]

ABSTRACT: The crystal structure of the closed form of citrate synthase, with citrate and CoA bound, from the hyperthermophilic Archaeon *Pyrococcus furiosus* has been determined to 1.9 Å. This has allowed direct structural comparisons between the same enzyme from organisms growing optimally at 37 °C (pig), 55 °C (*Thermoplasma acidophilum*) and now 100 °C (*Pyrococcus furiosus*). The three enzymes are homodimers and share a similar overall fold, with the dimer interface comprising primarily an eight α-helical sandwich of four antiparallel pairs of helices. The active sites show similar modes of substrate binding; moreover, the structural equivalence of the amino acid residues implicated in catalysis implies that the mechanism proceeds via the same acid−base catalytic process. Given the overall structural and mechanistic similarities, it has been possible to make detailed structural comparisons between the three citrate synthases, and a number of differences can be identified in passing from the mesophilic to thermophilic to hyperthermophilic citrate synthases. The most significant of these are an increased compactness of the enzyme, a more intimate association of the subunits, an increase in intersubunit ion pairs, and a reduction in thermolabile residues. Compactness is achieved by the shortening of a number of loops, an increase in the number of atoms buried from solvent, an optimized packing of side chains in the interior, and an absence of cavities. The intimate subunit association in the dimeric *P. furiosus* enzyme is achieved by greater complementarity of the monomers and by the C-terminal region of each monomer folding over the surface of the other monomer, in contrast to the pig enzyme where the C-terminus has a very different fold. The increased number of intersubunit ion pairs is accompanied by an increase in the number involved in networks. Interestingly, all loop regions in the *P. furiosus* enzyme either are shorter or contain additional ion pairs compared with the pig enzyme. The possible relevance of these structural features to enzyme hyperthermostability is discussed.

The Archaea are a phylogenetically distinct Domain of organisms that inhabit a diverse range of extreme environments. Phenotypically, they can be divided into a number of groups, including halophiles, methanogens, thermophiles, and psychrophiles (Woese *et al*., 1990). *Pyrococcus furiosus* is a hyperthermophilic Archaeon, growing optimally at 100 °C. Structural studies on homologous proteins from mesophilic and hyperthermophilic organisms may reveal intrinsic features necessary for the stabilization of proteins at high temperatures, and such knowledge may have a profound impact on our understanding of the fundamentals of protein stability and on the potential use of thermostable proteins in biotechnological processes.

For our comparative studies we have chosen the enzyme citrate synthase (E.C. 4.1.3.7) (Muir *et al*., 1994), which catalyzes the condensation of oxaloacetate and acetyl-CoA to form citrate and CoA.[1] There is a large database of known sequences for this enzyme, and crystal structures have been determined for the open (ligand-free) and closed (ligand-bound) forms of the enzyme from pig and chicken heart (Remington *et al*., 1982; Remington, 1992; Usher *et al*., 1995) and the open form from the thermophilic Archaeon *Thermoplasma acidophilum* (Russell *et al*., 1994), which grows optimally at 55 °C. *P. furiosus* citrate synthase (*Pf*CS) exists as a homodimer of $M_r = 81\,600$, with each monomer comprising 376 amino acids. The gene for the enzyme has previously been cloned, sequenced, and expressed in *Escherichia coli* and a purification scheme for the recombinant enzyme established (Muir *et al*., 1995).

The catalytic activities of the citrate synthases are similar at their normal operating temperatures. The V_{max} values, in micromoles of product formed per minute per milligram of protein, are 281 ± 23 for pigCS at 37 °C, 100 ± 14 for *Tp*CS at 60 °C, and 226 ± 12 for *Pf*CS at 90 °C. Although *Pf*CS has a growth optimum at 95−100 °C, the instability of oxaloacetate beyond 90 °C limits the assay to this temperature. These data suggest that there is a catalytic cost to be paid for thermostability. However, it may also be that there are physiological restrictions that place a limit on the cell's catalytic turnover rates.

The citrate synthases show thermal stabilities in line with the normal habitat temperatures of the organisms. Measurements on irreversible thermal denaturation give half-lives of 4.7 min for pigCS at 47 °C, 56.8 min for *Tp*CS at 70 °C, and 17.0 min for *Pf*CS at 100 °C. Clearly, *Pf*CS must contain additional intrinsic structural featues, compared to pigCS or *Tp*CS, which allow it to remain folded and active

[†] This work was supported by the Biotechnological and Biological Sciences Research Council (BTD Research Grant to M.J.D., D.W.H., and G.L.T., and a CASE studentship with Zeneca BioProducts to J.M.C.F.). Data collection at EMBL, Hamburg, was supported by the European Union through the HCMP Access to Large Installation Project, Contract CHGE-CT93-0040.

[‡] The atomic coordinates have been deposited in the Brookhaven Protein Data Bank with accession code 1AJ8.

* Corresponding author.

[⊗] Abstract published in *Advance ACS Abstracts,* July 15, 1997.

[1] Abbreviations: pigCS, pig citrate synthase; *Pf*CS, *Pyrococcus furiosus* citrate synthase; *Tp*CS, *Thermoplasma acidophilum* citrate synthase; CoA, coenzyme A.

S0006-2960(97)00532-1 CCC: $14.00 © 1997 American Chemical Society

at high temperatures. There is limited information on the thermodynamics of thermal unfolding for hyperthermophilic proteins, with no clear consensus on the expected values for ΔG of unfolding compared to mesophilic proteins which have typical ΔG values from 5 to 15 kcal/mol (Privalov, 1979). For thermostable proteins, the unfolding free energy curve may be shifted to higher temperatures or flattened without a change in maximum ΔG (Jaenicke, 1991; Vielle & Zeikus, 1996). In a recent study of the small (7 kDa) monomeric DNA-binding protein Sso7d from *Sulfolobus solfataricus* (growth optimum 80 °C), ΔG of unfolding has a maximum of 7 kcal/mol at 9 °C, falling to 2.8 kcal/mol at 80 °C and 1 kcal/mol at 100 °C, showing a reduced thermodynamic stability at higher temperatures (Knapp *et al*., 1996). Citrate synthase is a much larger protein and functions only as a dimer, suggesting that maintenance of its dimeric integrity at higher temperatures will be important. A full thermodynamic analysis of a range of citrate synthases from organisms living from 0 to 100 °C is required, although clearly to monitor the unfolding of a protein at temperatures >100 °C will involve specialized equipment.

*Pf*CS exhibits 30% sequence identity with pigCS and 42% identity with *Tp*CS. Insights into the basis of protein thermostability can be derived from sequence information alone (Menendez-Arias & Argos, 1989), but clearly there is a need to place any sequence differences into a structural context via structural determination of specific enzymes [for recent reviews, see Russell and Taylor (1995), Daniel *et al*. (1996), and Vieille and Zeikus (1996) and references therein)]. We now report the crystal structure of the closed form of citrate synthase from the hyperthermophilic archaeon *P. furiosus*, which allows direct structural comparisons between the same enzyme from organisms growing optimally at 37 °C (pig), 60 °C (*Tp. acidophilum)*, and now 100 °C (*P. furiosus*).

MATERIALS AND METHODS

Crystallization. The recombinant *Pf*CS was purified as detailed in Muir *et al.* (1995). Briefly, a cell extract of *E. coli* cells expressing the recombinant *Pf*CS was heat-treated at 85 °C for 15 min to denature most of the host proteins and was then subjected to affinity chromatography on a Matrex Red GelA column, with specific elution of the enzyme with oxaloacetate and CoA (James *et al.*, 1994). Fractions with citrate synthase activity were concentrated and buffer-exchanged in an Amicon Centriprep concentrator (30K cutoff). Crystals were grown by the hanging-drop, vapor-diffusion method at room temperature, using the Crystal Screen from Hampton Research as the precipitating agents. Crystals grew in the presence of 0.1 M sodium citrate and 1.0 M ammonium phosphate as the precipitating agent and at a protein concentration of 2 mg/mL in 20 mM Tris-HCl buffer (pH 8.0) containing 25 mM KCl.

Data Collection. Initial X-ray data were collected on a 300 mm MarResearch image plate mounted on an Enraf-Nonius X-ray generator operating at 45 kV and 80 mA. Diffraction extended to beyond 3.0 Å but was limited in-house to 3 Å by the long *c*-axis. The crystals belong to space group $P4_12_12/P4_32_12$ with $a = b = 99.5$ Å and $c = 243.0$ Å.

After the solution and refinement of the *Pf*CS structure to 3.0 Å (see below), a synchrotron data set to 1.9 Å resolution was collected from one crystal at 100 K on a 300 mm MarResearch image plate at station X-11, Hamburg, operating at a wavelength of 0.9083 Å. The crystal was soaked for 5 min in mother liquor containing 30% (v/v) glycerol as a cryoprotectant (Garman & Mitchell, 1996). Cell shrinkage was observed upon flash-freezing, with $a = b = 98.29$ Å and $c = 238.02$ Å.

Table 1: X-ray Data and Refinement Statistics of *Pf*CS

	1.9 Å data	3.0 Å data
observations	848543	150013
unique reflections ($F > 0\sigma$)	91136	23561
unique reflections ($F > 2\sigma$)	90047	22732
completeness (%) ($F > 0\sigma$)	98	96
completeness (%) (1.97−1.90)	98	
R_{merge} (%)	3.9	10.0
R_{merge} (%) (1.97−1.90)	15.9	
R-factor ($F > 2\sigma$) (%)	19.1	20.8
free *R*-factor ($F > 2\sigma$) (%)	23.2	26.2
R-factor ($F > 0\sigma$) (%)	19.4	21.5
free *R*-factor ($F > 0\sigma$) (%)	23.4	27.3
no. of protein atoms	5 690	5 690
no. of ligand atoms	116	116
no. of solvent atoms	482	
rmsd in bond lengths (Å)	0.006	0.014
rmsd in bond angles (deg)	1.72	1.66
av main chain *B*-factor (Å^2)	21.3	21.4
av main chain *B*-factor (Å^2) of large domain	19.9	19.0
av main chain *B*-factor (Å^2) of small domain	25.0	26.9

Data processing was performed using Denzo/scalepack (Otwinowski & Minor, 1997), with intensities being reduced to amplitudes using Bayesian statistics as implemented in the program TRUNCATE (CCP4, 1994) (Table 1).

Molecular Replacement. The structure of *Pf*CS was solved by the method of molecular replacement using the program AMoRE (Navaza, 1992) using the 3.0 Å data set. The volume of the asymmetric unit indicated that it contained one or two dimers. A search model was constructed which consisted of the *Tp*CS dimer superimposed on the pigCS dimer, both models were reduced to polyalanine, and the pig enzyme also had its first 35 and last 11 residues removed. The two models were used simultaneously in AMoRE. Results are discussed in terms of an AMoRE correlation coefficient (Navaza, 1992) with significance of peaks in terms of standard deviations above the mean. Using an outer Patterson cutoff radius of 25 Å and data in the resolution range of 20−4 Å, a list of 20 rotation function peaks was obtained with the top peak having an AMoRE correlation coefficient (CC) of 13.2 (3.26σ). A translation function, using data in the resolution range of 20−6 Å, in space group $P4_12_12$, gave a clear solution with a CC of 41.5 (8.72σ), which used the 14th highest peak in the rotation function [CC of 11.3 (2.79σ)]. The next highest solution of the translation function had a CC of 27.9 (4.72σ). A translation function in the enantiomorphic space group $P4_32_12$ gave a highest CC of 29.8 (4.87σ). Attempts were made to identify a position of a possible second dimer in the asymmetric unit of the crystal in space group $P4_12_12$. All attempts were unsuccessful, and a difference Fourier revealed no significant additional density, confirming that the asymmetric unit contained a single dimer of *Pf*CS. The crystals therefore have a relatively high (65%) solvent content. The dimer was then subjected to rigid-body refinement within AMoRE to give a CC of 52.9 and an *R*-factor of 51.8%. The solution gave no bad clashes with symmetry-related molecules in the unit cell.

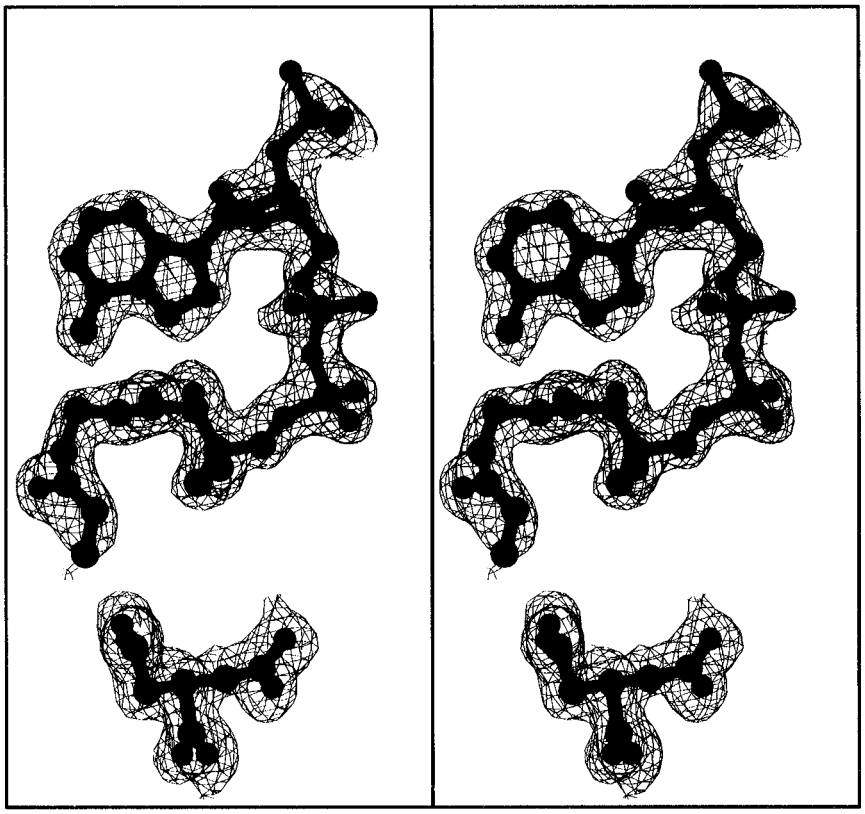

FIGURE 1: Stereo drawing of the 1.9 Å $2F_o - F_c$ electron density map around citrate and CoA in monomer A in *Pf*CS (contoured at 1σ). Produced using Molscript (Kraulis, 1991).

Refinement and Model Building. Electron density maps were significantly improved using the solvent flattening algorithm of Wang or 2-fold noncrystallographic real space averaging using RAVE (Kleywegt & Jones, 1994a). Using a polyalanine *Tp*CS monomer as an initial model, side chain atoms were built and deviations of the main chain were modeled using the program O (Jones *et al*., 1991). Refinement was undertaken using X-PLOR (version 3.1) (Brünger *et al.*, 1987, 1990) via a standard simulated annealing protocol, but due caution was observed throughout since the data extended, initially, to only 3.0 Å. The free *R*-factor (Brünger, 1992) was used, and its change, rather than that of the conventional *R*-factor, was always used to monitor the refinement. Tight noncrystallographic symmetry restraints between the two monomers of the dimer were maintained throughout the refinement, using a weight of 400 kcal mol^{-1} $Å^{-2}$. Citrate and CoA were also modeled into the observed density. CoA was present in the active site from its use in the purification of *Pf*CS. A final round of positional refinement was undertaken with the large and small domains acting as individual groups in the noncrystallographic symmetry restraints, followed by grouped *B*-factor refinement. The final free *R*-factor for the model is 27.3% and the *R*-factor 21.5% ($F > 0\sigma$), with rms deviations for bond lengths and bond angles being 0.014 Å and 1.66°, respectively (Table 1). A Ramachandran plot reveals that 91% of residues lie in the most favored regions and none in disallowed regions. All residues lie in acceptable environments as judged by a 3D−1D profile plot (Luthy *et al*., 1992). The initial four residues at the N-terminus are not included in the final model due to poorly defined electron density.

Refinement of the 1.9 Å Structure. The 3.0 Å structure was initially subjected to cycles of rigid-body refinement, using X-PLOR version 3.851, using data in the resolution range of 15−4 Å. This resulted in an *R*-factor of 34.2% ($R_{free} = 36\%$). A bulk solvent correction was applied to the data (Jiang & Brünger, 1994), and an initial round of simulated annealing refinement to 2.5 Å reduced the *R*-factor to 29.3% ($R_{free} = 33.3\%$), after individual *B*-factor refinement. No ncs restraints were applied throughout refinement due to the high observation:parameter ratio present in the data. Manual rebuilding and refinement to 1.9 Å decreased the *R*-factor to 24.7% ($R_{free} = 30.0\%$). Sigmaa-weighted $2F_o - F_c$ electron density maps were calculated, and solvent molecules were identified using the "waterpick" algorithm within X-PLOR. The model was manually modified using O and subjected to further rounds of refinement using data in the resolution range 100−1.9 Å. The current *R*-factor is 19.4% and R_{free} is 23.4% ($F > 0\sigma$), with rms deviations for bond lengths and bond angles being 0.006 Å and 1.72°, respectively (Table 1). Figure 1 shows the quality of the electron density map at 1.9 Å around the citrate and CoA. A Ramachandran plot reveals that 94% of residues lie in the most favored regions and none in disallowed regions. All residues lie in acceptable environments as judged by a 3D−1D profile plot (Luthy *et al*., 1992). The initial five residues at the N-terminus are not included in the final model of either monomer and the final C-terminal residue of one monomer due to poorly defined electron density.

RESULTS

*Overall Structural Comparisons. Pf*CS exists as a dimer of identical monomers, with each monomer composed of 16 α-helices distributed between a large and a small domain

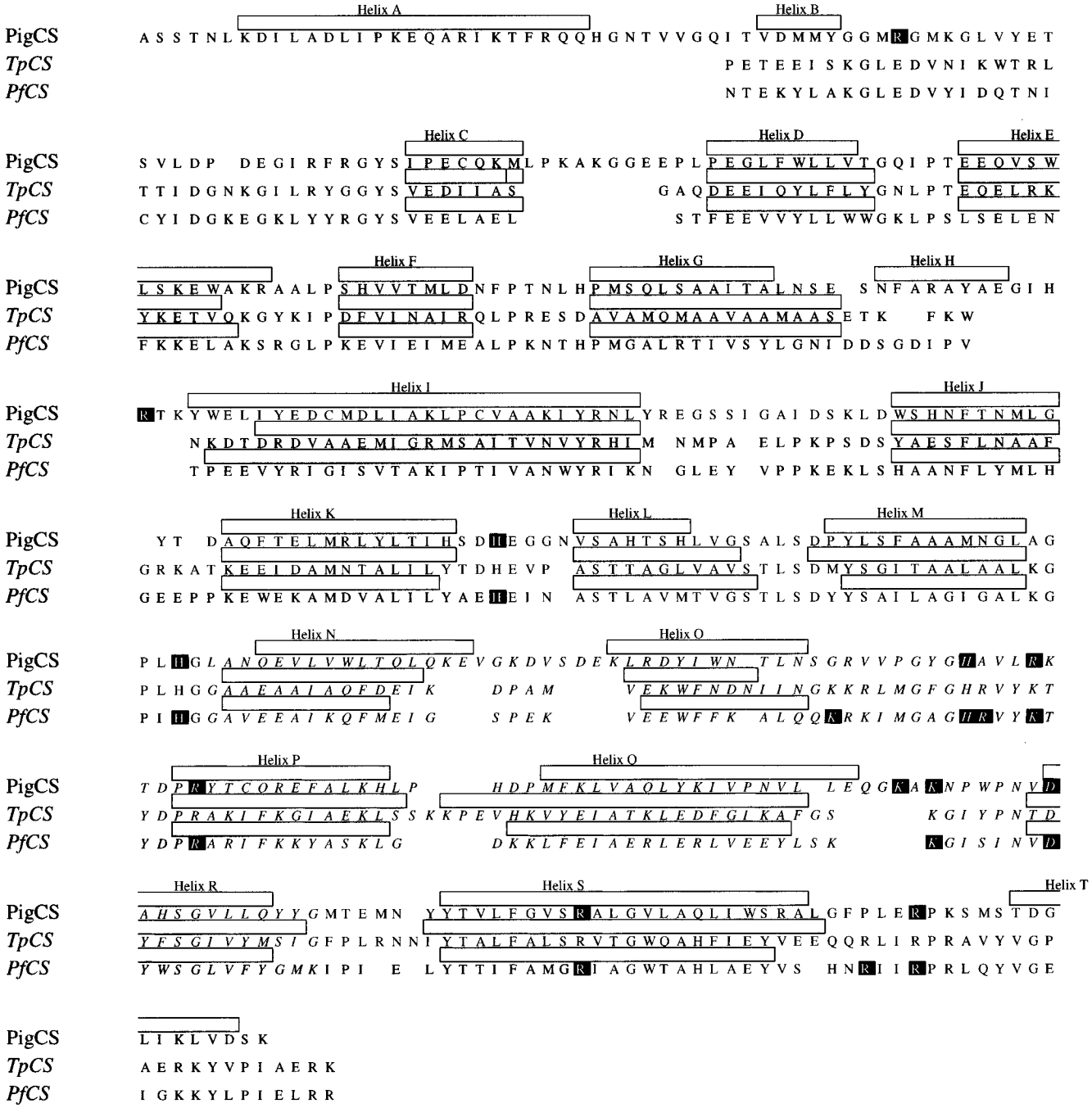

FIGURE 2: Structure-based sequence alignment of pigCS, *Tp*CS, and *Pf*CS. α-Helices for pigCS, *Tp*CS, and *Pf*CS are indicated by lines above their respective sequence. Active site residues are highlighted in inverse type for pigCS and *Pf*CS. Residues in the small domain are italicized. Produced using Alscript (Barton, 1993).

[helices C−G and I−S, following the nomenclature of Remington *et al.* (1982)]. The reduction in the number of helices compared with pigCS (20 helices) is due to the absence of helices A, B, H, and T (Figure 2). Both archaeal enzymes are shorter than the eukaryotic enzyme with pigCS, *Tp*CS, and *Pf*CS containing 437, 384, and 376 residues per monomer, respectively. *Pf*CS also contains two small 3_{10} helices at the N- and C-termini (residues 7−11 and 371−375). PigCS contains a small section of antiparallel β-sheet formed by residues 56−69. This secondary structural unit is also present in *Pf*CS (residues 20−36), but an additional section of intersubunit parallel β-sheet is also formed between the N-terminus of one monomer and the C-terminus of the other monomer (residues 14−18 and 358−362). Superposition of the closed form of *Pf*CS onto the closed form of pigCS reveals a root mean square deviation (rmsd) of 2.19 Å for 356 Cα atoms. In pigCS, the small domain (helices N−R) is known to rotate relative to the large domain upon binding of substrates. The relative orientation of the two domains in the closed form of *Pf*CS is very similar to that in pigCS. The average main chain *B*-factor for the small domain is higher than that of the large domain (Table 1), indicating increased flexibility of the small domain with respect to the large domain, a feature observed previously in both pigCS and *Tp*CS. In comparing the overall structures of the two archaeal enzymes, it should be noted that, at present, we have only the structures of the closed form of *Pf*CS and the open form of *Tp*CS. However, superposition of the large domains of *Pf*CS and *Tp*CS shows a rmsd of 0.88 Å for 251 Cα atoms, and superposition of the small

domains shows a rmsd of 0.57 Å for 95 Cα atoms. This reflects the fact that the sequence identity between the small domains is 53% compared with only 39% between the large domains.

Common to the dimeric citrate synthases, the monomer−monomer association remains an eight α-helical sandwich, comprising four antiparallel pairs of helices (F, G, L, and M). However, dramatic differences between the folds of the pigCS, *Tp*CS, and *Pf*CS occur at the N- and C-termini. In pigCS, the N-terminus forms a long helix (residues 7−27), which, for the main part, extends over the surface of the monomer to which it belongs. Both *Pf*CS and *Tp*CS are 35 residues shorter at the N-terminus compared with pigCS (Russell *et al*., 1994; Muir *et al*., 1995). The C-terminus of *Pf*CS adopts a totally different fold from that in pigCS (Figure 3). That is, it is four residues longer that the pigCS C-terminus, and it folds in an extended form over the surface of the other monomer to give the appearance of monomers embracing one another (Figure 3a), whereas it forms a small helical region in pigCS.

It should be noted that the density of the five amino acids at the N-terminus of the *Pf*CS was too weak to be interpreted, a similar situation being found in the *Tp*CS crystal structure (Russell *et al*., 1994). These observations may reflect a flexibility in the N-terminal region of the two proteins, although this would be surprising in view of the general overall compactness of the hyperthermophilic citrate synthase as detailed below.

The Active Site. (i) Citrate Binding. Citrate binds in an analogous manner to that previously observed in pigCS, via the interactions with three arginine side chains (271, 337, and 356′, where the prime on the amino acid denotes a residue on the other monomer of the dimer) and three histidines (188, 223, and 262) (Figures 1 and 4). The structural location of these residues is identical in the *Pf*CS and pigCS.

(ii) CoA Binding. PigCS provides three arginine ligands for the three phosphate groups of CoA (Arg 324 and Arg 46 for the α- and β-phosphates and Arg 164′ for the 3′-phosphate). Two lysine residues (366 and 368) are also in the vicinity of the disphosphate. *Pf*CS also provides ligands for these phosphates, but their structural location is distinctly different: Arg 164′ in pigCS is located in the H−I loop of the second monomer, but this loop is dramatically shortened in *Pf*CS. Instead, the 3′-phosphate of CoA interacts with Lys 254 and Lys 305 in *Pf*CS, both located on the small domain of the molecule. The α- and β-phosphates interact with Arg 263, Lys 266 (structurally equivalent to Arg 324 in pigCS), and Arg 353′ in *Pf*CS. Therefore, in both enzymes, one ligand comes from the second subunit. Recognition of the rest of the CoA molecule is very similar in both enzymes (Figures 1 and 4) and involves hydrogen bonds to main chain atoms of the protein. The terminal C and S atoms of CoA are not visible in the electron density; such was the situation in the crystal structure of pigCS complexed with citrate and CoA (Remington *et al.*, 1982).

(iii) Catalytic Residues. His 274, His 320, and Asp 375 (pigCS numbering) have been implicated crystallographically (Usher *et al*., 1995) and by mutagenesis experiments (Alter *et al*., 1990; Kurz *et al*., 1995) to play a central role in the mechanism of action in pigCS. His 223, His 262, and Asp 312 are the structurally equivalent residues in *Pf*CS. Therefore, the catalytic mechanism is likely to be the same in both enzymes, via concerted acid−base catalysis.

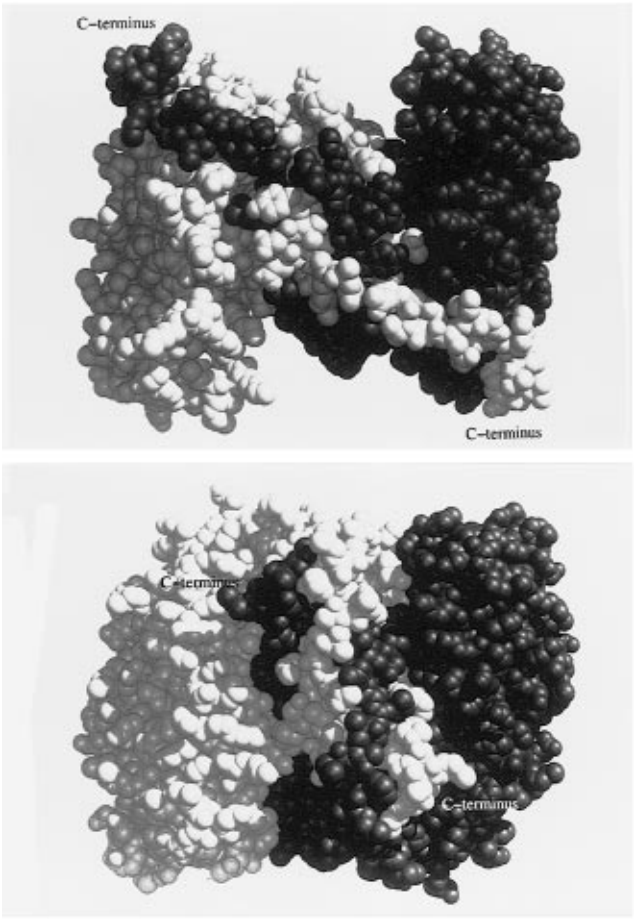

FIGURE 3: (a, top) Space-filling representation of the *Pf*CS dimer highlighting the C-terminal residues of each monomer wrapping around the other monomer. (b, bottom) Space-filling representation of the pigCS dimer [orientation as in (a)]. Produced with MidasPlus (Ferrin *et al*., 1988; Huang *et al*., 1991).

(iv) Active Site Water Structure. PigCS has seven water molecules within a 10 Å sphere of the citrate/oxaloacetate molecule, all buried from bulk solvent. Six of these water molecules are highly conserved in *Pf*CS, with the position of the remaining one being occupied by the OH group of Tyr 265. This level of conservation between enzymes from such diverse organisms suggests a possible integral role of water, and its positioning, in the catalytic mechanism.

Structural Differences between Mesophilic and Thermophilic Citrate Synthases. Given the overall similarity in the folds, active sites, and subunit interfaces of the citrate synthases, detailed structural comparisons can now be made between the same protein from a mesophile (pigCS, 37 °C), a thermophile (*Tp*CS, 60 °C), and a hyperthermophile (*Pf*CS, 100 °C). Care has to be taken when including *Tp*CS in the comparisons between the "closed" (liganded) forms of the *Pf*CS and pigCS, since only the structure of the "open" (unliganded) form of the *Tp*CS is known. Nevertheless, structural regions unaffected by the conformational change induced by substrate binding, for example, subunit interface interactions, can be included in direct comparisons between the three enzymes.

(a) Loops. *Tp*CS has four loops that are significantly shorter than those in the pigCS, between helices C → D, G → I (involving the complete deletion of helix H),

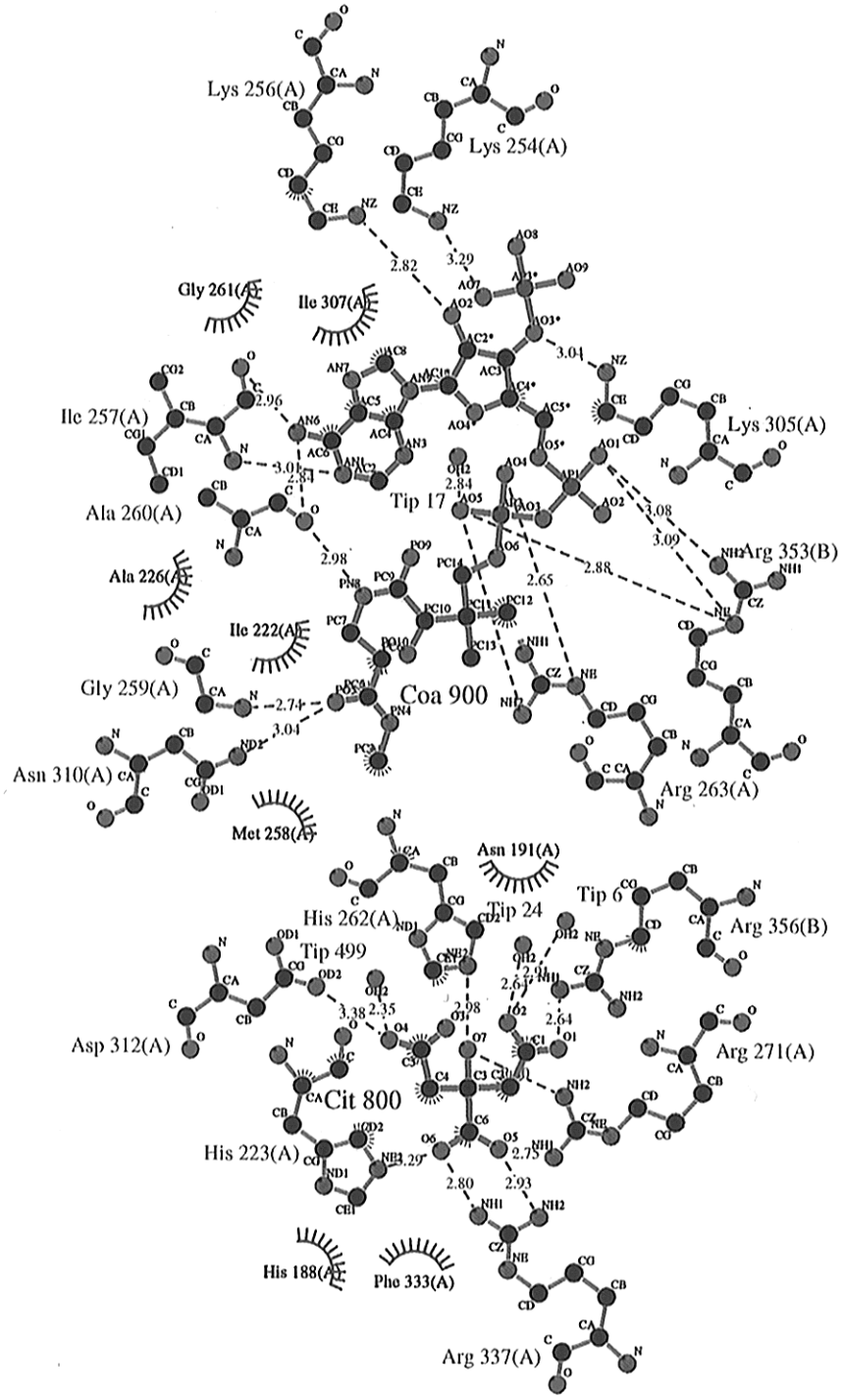

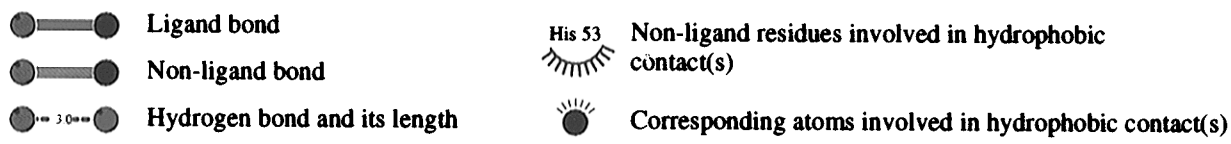

FIGURE 4: Details of binding of citrate and CoA to monomer A of *Pf*CS. Produced using LIGLOT (Wallace *et al.*, 1995).

N → O, and Q → R. *Pf*CS has these same four short loops and a further two loops that are shortened compared to both the pigCS and *Tp*CS, between helices P → Q and R → S (Figure 1).

(b) Cavities. Detection of cavities capable of accommodating a water molecule was undertaken using VOIDOO (Kleywegt & Jones, 1994b) with a 1.4 Å probe and a 0.75 Å grid. The cavity calculations were carried out on the dimer of *Pf*CS, using the multirotational approach suggested by Kleywegt and Jones (1994b) in order to reduce errors caused by the grid specifications. It was previously reported that the number and size of internal cavities in the open *Tp*CS were fewer than in the open pigCS: three cavities with a volume of 211 Å^3 compared with seven with a volume of

Table 2: Variation in Size and Internal Packing of PigCS, *Tp*CS, and *Pf*CS[a]

	pigCS closed	pigCS closed (N-terminus deleted)	*Pf*CS closed	pigCS open	*Tp*CS open
volume × 10^4 (Å^3)	9.98	9.18	8.65	9.96	8.71
accessible surface area (Å^2)	31700	29900	27205	33400	30200
atoms buried (%)	53.1	52.0	54.0	50.1	50.7

[a] Closed refers to the enzyme conformation with citrate and CoA bound, and open refers to the nonliganded conformation of the enzyme. Two sets of data are given for the closed conformation of the pigCS, first for the whole molecule and second with the first 35 residues of the N-terminus deleted from the model. Accessibility calculations were performed on the citrate synthase dimers with GRASP (Nichols *et al*., 1991) and volume calculations with VOIDOO (Kleywegt & Jones, 1994b).

612 Å^3, respectively (Russell *et al*., 1994). Calculations with the closed pigCS reveals four cavities with a volume of 304 Å^3, whereas the closed *Pf*CS does not contain any cavities. The two largest cavities present in the pigCS monomer (present in both open and closed forms) are filled by single amino acid replacements in both *Tp*CS and *Pf*CS. Ala 118 in pigCS is replaced by Tyr 76 in *Tp*CS and Arg 75 in *Pf*CS, and Ser 412 in pigCS is replaced by Tyr 355 in *Tp*CS and Tyr 348 in *Pf*CS.

(c) Accessible Surface Area and Volume. *Pf*CS has a reduced accessible surface area and volume compared to pigCS (Table 2), and the percentage of atoms buried is also greater. It must be noted that these differences are not due solely to the N-terminal extension present in the pigCS, since identical calculations for an N-terminally deleted (35 residues) pigCS show *Pf*CS still to be significantly more compact (Table 2). Comparing the open form of *Tp*CS with the open form of pigCS, the thermophile is also more compact than the mesophile.

(d) Monomer−Monomer Association. The monomer−monomer association is composed of two parts: the eight-helix sandwich, which is the main component, and the interaction of the C-terminus of one monomer with the other monomer. First, the complementarity of packing of the two monomers can be viewed in terms of a gap volume index, defined as the gap volume between the two monomers divided by the interface accessible surface area (Jones & Thornton, 1995). The gap volume index is 1.86 for pigCS and 1.17 for the *Pf*CS, a lower figure being indicative of closer packing. The gap volume index for *Tp*CS is 1.10, but the final 14 C-terminal residues (which form an extensive set of intersubunit interactions in the *Pf*CS) are not present in the final model of *Tp*CS, due to poorly defined electron density. If the gap volume index is recalculated for a C-terminally deleted model of the hyperthermophilic enzyme, a figure of 1.02 is obtained. The nature of the subunit interface is discussed in (*e*).

As described above, with respect to the C-terminal interactions, in *Pf*CS the C-terminus of one monomer wraps around the other monomer, clasping the two together in an intimate embrace (Figure 3). An ion pair between Arg 375 (the penultimate residue) and Glu 48′ may also strengthen this association. In a study of a different crystal form of *Pf*CS, albeit at a lower resolution than this study (3.5 Å, unpublished results of the authors), where citrate was not present, the C-terminus was not defined in the electron density. In addition, the C-terminus of the open form of *Tp*CS was not observed in the electron density despite the high sequence similarity to *Pf*CS, including the two residues forming the terminal ion pair in *Pf*CS. Therefore, it may be that the C-terminus only becomes ordered upon substrate binding, thereby stabilizing the closed form of the enzyme.

Table 3: Ion Pairs in Citrate Synthase[a]

	pigCS	*Tp*CS	*Pf*CS
6 Å cutoff			
total ion pairs	82 (315)	90 (318)	105 (376)
intra ion pairs in A	35 (124)	39 (132)	42 (119)
intra ion pairs in B	35 (124)	41 (137)	39 (115)
inter A to B	12 (67)	10 (48)	24 (142)
5 Å cutoff			
total ion pairs	64 (271)	65 (252)	69 (294)
intra ion pairs in A	26 (102)	30 (109)	25 (82)
intra ion pairs in B	26 (102)	29 (107)	24 (83)
inter A to B	12 (67)	6 (35)	20 (128)
4 Å cutoff			
total ion pairs	36 (185)	43 (184)	43 (217)
intra ion pairs in A	12 (59)	21 (81)	14 (50)
intra ion pairs in B	12 (59)	18 (76)	12(47)
inter A to B	12 (67)	4 (27)	17 (119)
involvement			
Arg	22/38 (58%)	19/34 (56%)	24/33 (73%)
Lys	18/50 (36%)	30/54 (56%)	29/64 (45%)
His	10/28 (36%)	8/12 (67%)	6/16 (38%)
Glu	28/48 (58%)	29/50 (58%)	43/76 (57%)
Asp	20/42 (48%)	16/38 (42%)	9/22 (41%)

[a] The number of ion pairs is given using a 6, 5, and 4 Å cutoff distance between charged groups. An estimate of the Coulomb energy assuming a distance-dependent dielectric is given in parentheses. This was calculated as $332.06/(Dr_{ij})$, in kcal/mol, where D is the distance of the center of the ion pair from the center of mass of the dimer, in Å, and r_{ij} is the distance between the ions, in Å. The percent involvement in ion pairs of charged amino acids is calculated using the 5 Å cut-off distance. A and B refer to the two monomers of the native dimer.

Both the N- and C-termini are involved in intersubunit contacts in *Pf*CS, whereas the first 25 and the final 10 residues in pigCS exhibit no interaction with the other subunit.

(e) Ion Pairs. Table 3 presents the number of ion pairs observed in pigCS, *Tp*CS, and *Pf*CS, identified using cutoff distances between oppositely charged residues of 4 Å (Barlow & Thornton, 1983), 5 Å, and 6 Å. The major difference between the hyperthermophile and mesophile is a consistently significant increase in intersubunit ion pairs observed in the hyperthermophilic citrate synthase compared with the mesophilic enzyme (Figure 5), whereas no significant increase is observed in *Tp*CS compared with pigCS. Also, even upon introduction of a larger cutoff distance (6.0 Å) the number of intersubunit ion pairs in pigCS does not change, whereas the number of possible ion pairs increases in *Pf*CS.

Many of the additional intersubunit ion pairs in *Pf*CS compared with pigCS are located primarily in helix G and helix M which make up the central four helices of the eight-helical sandwich of the subunit interface, with helices F and L the outer four helices (Figure 6a). Residues His 93′, Arg 99′, Asp 113, Asp 206, and Lys 219′, from both subunits, form a five-membered ion pair network at each end of these

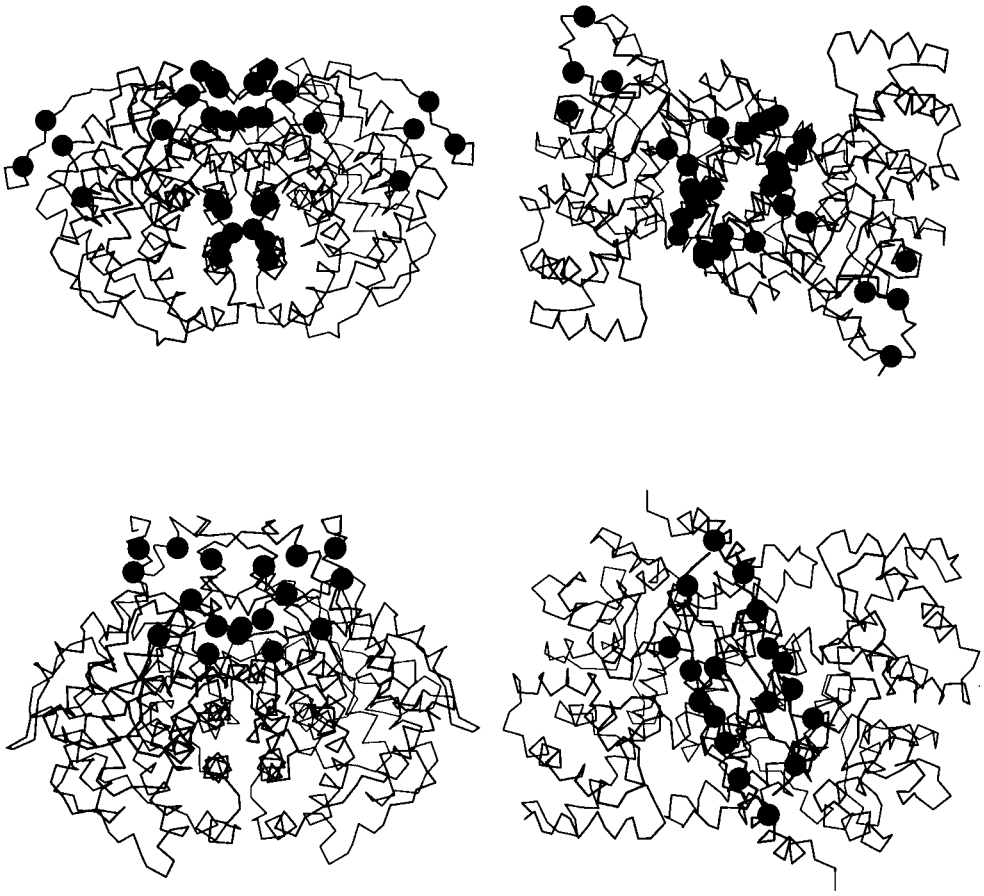

FIGURE 5: Orthogonal views of intrasubunit ion pair interactions in *Pf*CS (top panels) and pigCS (bottom panels). The Cα atoms of residues involved in intersubunit ion pairs are displayed in CPK representation. Solid circles denote a glutamic acid or aspartic acid residue and an arginine, lysine, or histidine residue. Produced using Molscript (Kraulis, 1991).

helices. The lack of these ion pairs in pigCS is apparent in Figure 5, bottom left panel. A further two four-membered intersubunit ion pair networks are also present in *Pf*CS (residues Asp12, Glu 189, Arg 356, and Arg 358). Helix G was previously proposed to be the site of an important difference between the subunit interfaces of pigCS and *Tp*CS, a trend toward hydrophobicity being observed in the thermophilic enzyme where the number of alanines increased from 3 to 8 (Russell *et al*., 1994). Therefore, the structure of the hyperthermophilic citrate synthase has revealed an alternative approach to maintaining dimeric integrity at high temperatures. Also, an intersubunit ion pair is located at both the N-terminus (Lys 8−Asp 16′) and the C-terminus (Glu 48−Arg 375′). A four-residue intersubunit network present in pigCS (Asp 420 and His 246) is replaced by a hydrophobic cluster in *Pf*CS, comprising a high percentage of isoleucine residues (see later), surrounded by a complete ring of intersubunit ion pairs (Figure 6b).

A number of the ion pairs in the *Pf*CS are located in loop regions, such that in all nonhelical regions of the hyperthermostable enzyme either extra ion pairs are present or the loop regions connecting the helices are shorter compared with the mesophile.

(f) Hydrogen Bonds. The number of hydrogen bonds was calculated using HBPLUS (McDonald & Thornton, 1994) on the dimeric forms of each enzyme. PigCS, *Tp*CS, and *Pf*CS have an average of 0.99, 0.97, and 0.98 H-bonds per residue, respectively, showing no significant difference in hydrogen bonding between the three enzymes. The number of charge-neutral hydrogen bonds in the three enzymes also shows little difference, with pigCS, *Tp*CS, and *Pf*CS having an average of 0.37, 0.29, and 0.33 per residue, respectively. However, an increase in intersubunit H-bonds, 51 compared to 40, is observed in *Pf*CS compared with pigCS.

(g) Proline in β-Turns. Pig*CS* contains 8 prolines in 21 β-turns, *Tp*CS has 2 in 16, and *Pf*CS has 4 in 18.

(h) Helix Capping. The three citrate synthases are almost entirely α-helical, yet there were no significant differences in the extent of helix capping, where the inherent dipole at the N-terminus was cancelled by the presence of a negatively charged residue (Richardson & Richardson, 1988). PigCS has 11 such caps (at Ncap, N1, or N2, where Ncap is the residue preceding the first residue, N1, of the helix), *Tp*CS also has 11, and *Pf*CS has 9.

(i) Thermolabile Residues. Of the 20 amino acids, Asn, Gln, Met, and Cys can be classed as thermolabile due to their tendency to undergo deamidation or oxidation at high temperatures and therefore may be naturally discriminated against in thermostable proteins. A trend is observed that follows the expected pattern; pigCS has 18 Asn (4.1%), 17 Gln (3.9%), 15 Met (3.4%), and 4 Cys (0.9%), *Tp*CS has 15 Asn (3.9%), 10 Gln (2.6%), 12 Met (3.1%), and 0 Cys (0%), and *Pf*CS contains 11 Asn (2.9%), 5 Gln (1.3%), 9 Met (2.4%), and 1 Cys (0.3%), These changes can now be put into a structural context. On eight occurrences, an Asn or Gln in pigCS is changed to a charged residue in *Pf*CS that now forms an ion pair, with only a single example of the reverse. *Tp*CS has five such replacements, with two

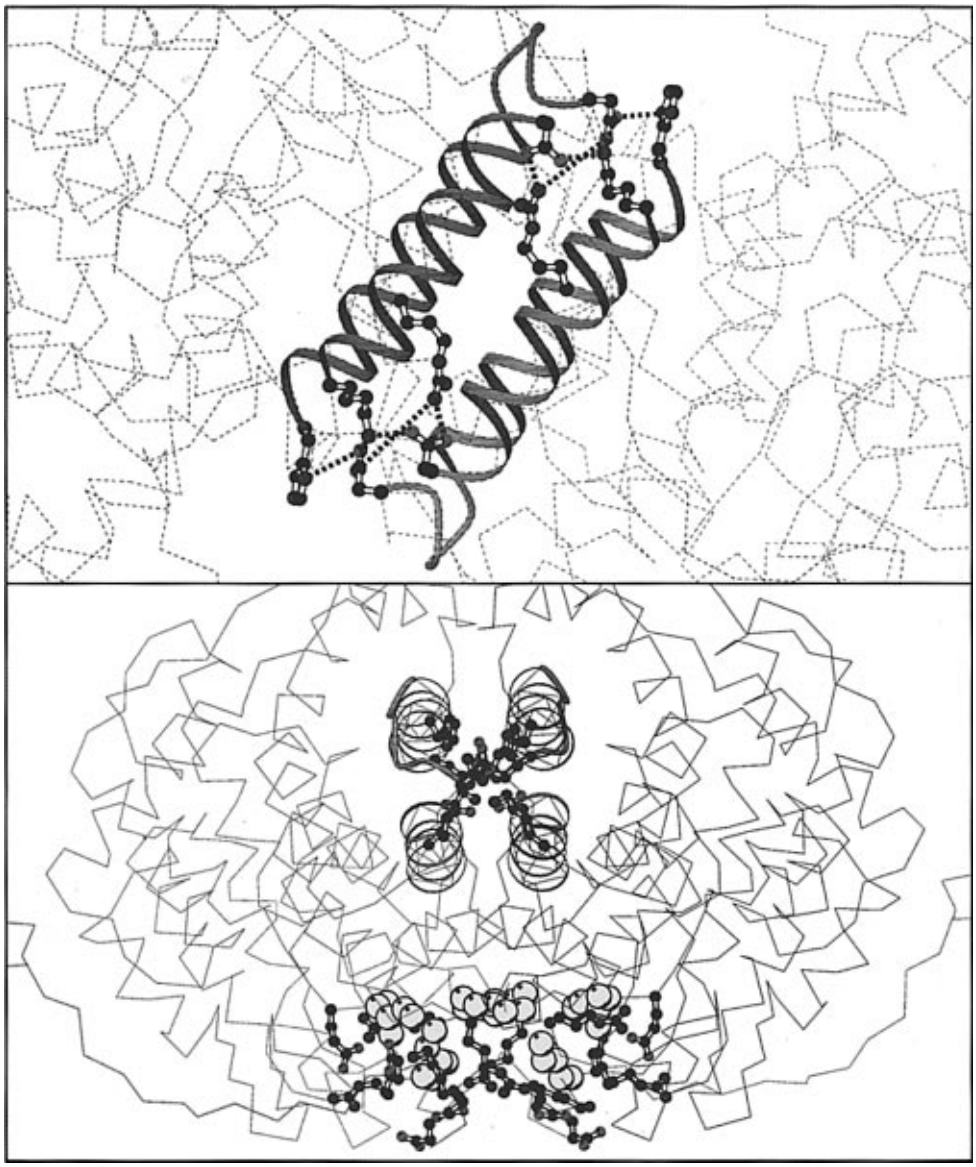

FIGURE 6: (a, top) Five-membered intersubunit ion pair networks in *PfCS*, viewed down the 2-fold axis of the dimer. Equivalent helices (G and M) from each monomer are colored similarly. (b, bottom) Orthogonal view of (a), highlighting the two five-membered intersubunit ion pair networks, the ring of intersubunit ion pairs, and the six-membered isoleucine cluster (colored in yellow). Produced using Molscript (Kraulis, 1991).

examples in the reverse direction. *Pf*CS and *Tp*CS also eliminate three and two thermolabile residues, respectively, via loop shortening. In the case of methionines, not only has *Pf*CS proportionately fewer methionines but they are all effectively buried from solvent in contrast to pigCS and *Tp*CS which have more methionines, many of which are exposed.

(j) Isoleucine Clusters. A significant increase in the number of isoleucine residues is observed in *Pf*CS compared with pigCS. These substitutions result in the formation of isoleucine clusters sandwiched between the intersubunit helices (F, G, L, and M) and helices I and S in each monomer. A cluster of six isoleucines (15, 190, and 355 from both monomers) forms a hydrophobic cluster inside the ion pair ring (see above and Figure 6b). Ile15 and Ile355 are conserved in *Tp*CS.

DISCUSSION

The crystal structure of *Pf*CS has enabled a direct structural comparison to be made between the same enzyme from organisms growing optimally at 37, 60, and 100 °C. The enzymes from the two Archaea, *Tp. acidophilum* and *P. furiosus*, are both recombinant proteins, although we have not been able to detect significant structural or functional differences between these and the nonrecombinant counterparts (Muir *et al.*, 1994, 1995). Furthermore, on the basis of an Arrhenius analysis of the respective rates of irreversible thermal inactivation (Muir *et al.*, 1995), the three citrate synthases have thermostabilities commensurate with the growth temperatures of their host organisms. Thus, the overall structural homology, including that of the active site and the mode of substrate binding, permits the identification of structural trends in going from the mesophilic to thermophilic to hyperthermophilic protein. These trends can now be discussed in the context of the differing stabilities of the citrate synthases and in particular the structural basis of hyperthermostability.

Of all the structural features analyzed, three trends that may contribute to thermostability in citrate synthase feature

prominently: compactness, an increase in number and nature of intersubunit ion pairs, and a reduction in thermolabile residues.

Compactness. An increase in compactness with increase in thermostability is achieved through several routes: shorter loops, a reduction in cavities, and greater surface complementarity at the dimer interface, all of which lead to a greater percentage of atoms buried from solvent. A tighter internal packing may be achieved through the formation of isoleucine clusters.

Shorter Loops. Both *Pf*CS and *Tp*CS have a number of shorter loops compared with pigCS. This observation, that the higher the growth temperature of the organism the shorter the protein loops, is consistent with high temperature molecular dynamic simulations on bovine pancreatic trypsin inhibitor, which revealed that loop and turn regions are likely to be the part of the structure that unfolds first during thermal denaturation (Daggett & Levitt, 1993). However, a multiple sequence alignment of all known citrate synthase sequences based on the crystal structures of pigCS, *Tp*CS, and *Pf*CS shows that a number of nonthermostable citrate synthases may also contain such shorter loops, although not to the same extent as observed in the thermophilic enzymes. Nevertheless, a number of other thermostable proteins, e.g., 1[4Fe-4S]ferredoxin from *Thermotoga maritima* (Macedo-Ribeiro *et al.*, 1996) and a thermostable endocellulase (Sakon *et al.*, 1996) do show reduced size of loop regions, indicating a possible role in protein thermostability.

Fewer Cavities. Cavity filling/forming mutations have highlighted the important role of internal packing in protein stability (Eriksson *et al.*, 1992; Richards & Lim, 1993), and therefore the absence of large cavities in *Pf*CS may contribute to its hyperthermostability by eliminating areas in the structure where nonoptimal packing occurs. A decrease in size and number of cavities was also noticed in the thermophilic triose-phosphate isomerase from *Bacillus stearothermophilus* compared with the same enzyme from mesophilic sources (Delboni *et al.*, 1995). A high degree of internal packing was also observed in the thermostable protein ecotin (Shin *et al.*, 1996).

Greater Surface Complementarity at the Dimer Interface. The improved complementarity of the monomers at the eight-helix interface in going from pigCS to *Tp*CS to *Pf*CS, as revealed by the gap volume index calculations, once again follows a trend as the growth temperature of the organism increases. This improved complementarity may allow the two monomers to remain associated in an intact dimer at high temperatures through optimized packing interactions. Dimer to monomer dissociation is thought to be the initial step in the thermal inactivation of pigCS (McEvily & Harrison, 1986).

The C-terminus of *Pf*CS differs significantly from that observed in pigCS, resulting in extensive monomer−monomer interactions. Citrate synthase is only active as a dimer since residues from both monomers participate in the active sites, and therefore the embracing of one monomer by the C-terminus of the other monomer may be necessary for dimer integrity at high temperatures. Additionally, in a manner analogous to that discussed above for loop regions, polypeptide termini tend to be flexible regions of proteins, and the involvement of the C-terminus of *Pf*CS in monomer−monomer contacts may reduce this flexibility and the consequent susceptibility to thermal denaturation. Similar additional interactions at the termini have been previously proposed to be an important contributor to thermostability of other proteins (Day *et al*., 1992; Starich *et al*., 1996), by reducing the fraying in these regions. However, the possible flexibility at the N-terminus of *Pf*CS and *Tp*CS remains surprising in this respect.

Interestingly, the C-terminus of *Pf*CS appears to be ordered only in the presence of substrates, which in turn increase the thermostability of both this enzyme and the *Tp*CS (in the presence of 5 mM citrate and 1 mM CoA, the first-order rate constants for irreversible thermal inactivations are decreased 12-fold for PfCS at 103 °C and 15-fold for TpCS at 91 °C). PigCS is also more thermostable in the presence of these ligands (the rate constant for inactivation being reduced 4-fold at 45 °C), which induce the closed conformation and thereby reduce the accessible surface area and increase the number of atoms buried. Significantly, both *Tp*CS and *Pf*CS have a lower accessible surface area and a higher number of atoms buried than the mesophilic enzyme.

Isoleucine Clusters. The high percentage of isoleucines in *Pf*CS results in the formation of a number of isoleucine clusters in the core of the protein. Such clusters were also observed in another hyperthermostable enzyme, glutamate dehydrogenase from *P. furiosus* (Yip *et al.*, 1995). Isoleucine may be favored over leucine in the formation of hydrophobic clusters due to the ability to exist in all three χ_1 angles compared to predominantly two for leucine side chains, thus enabling a tighter packing in the core of the molecule and enhancing van der Waals interactions.

The low accessible surface area and high percentage of atoms buried, maximizing internal packing interactions in *Pf*CS, have also been noticed in another hyperthermophilic enzyme structure, aldehyde ferredoxin oxidoreductase from *P. furiosus* (Chan *et al.*, 1995). Although in this case no mesophilic counterpart is known, a comparison was made with a test set of other globular proteins of similar size to provide a measure of the enzyme's relative size. More recently, the structure of the TATA-box binding protein from *P. furiosus* has been elucidated, and this enzyme also shows a similarly compact nature. In contrast, the crystal structures of the hexameric glutamate dehydrogenase from *P. furiosus* (Yip *et al*., 1995) and monomeric indole-3-glycerol phosphate synthase from *S. solfataricus* (growth temperature ≈ 80 °C) (Hennig *et al*., 1995) do not show such a marked trend toward compactness when compared with their mesophilic equivalents. Therefore, a very compact/well-packed protein does not seem to be a universal prerequisite for hyperthermostability.

Ion Pairs. The importance of surface ion pairs in determining protein thermostability was first highlighted by Perutz and Raidt (1975), while comparing ferredoxin and hemoglobin structures, and was subsequently proposed to be involved in stabilizing a number of other thermostable proteins (Walker *et al*., 1980; Korndörfer *et al*., 1995). There is an increase in the number of *intersubunit* ion pairs in *Pf*CS, and their involvement in complex networks mirrors that observed in the recently reported structure of the hyperthermophilic *P. furiosus* glutamate dehydrogenase (Yip *et al*., 1995). The presence of ion pair networks was also observed in *S. solfataricus* indole-3-glycerol phosphate synthase (Hennig *et al*., 1995) and the TATA-box binding protein

from *P. furiosus* (DeDecker *et al.*, 1996). The presence of networks of ion pairs may be energetically favorable due to the shared entropic cost upon ion pair formation (Nakamura, 1996).

The positioning of ion pairs is also crucial. Loop or random coil regions of a protein tend to be the most flexible areas and probably are the most likely to deform at high temperatures. All loop regions of *Pf*CS are altered with respect to pigCS by either loop shortening or increased ion pair interactions. A similar strengthening of loop regions was also observed in *S. solfataricus* indole-3-glycerol phosphate synthase (Hennig *et al.*, 1995).

Thermolabile Residues. An additional factor in an understanding of the structural basis of thermal stability may be the avoidance of thermolabile residues such as Asn, Gln, and Cys (Hensel, 1993). Both *Pf*CS and *Tp*CS have a lower number of these residues compared with pigCS as revealed by sequence analysis. The structural consequences of their replacement in *Pf*CS and *Tp*CS are, in many instances, to create additional electrostatic interactions. Thus the effect of their replacement is 2-fold: first, elimination of potential points of deamidation or oxidation and, second, introduction of new stabilizing interactions.

Other Features. It has been suggested that structural features such as hydrogen bonding, helix capping (Fersht & Serrano, 1993), and proline-stabilized turns (Watanabe *et al.*, 1994) may contribute to protein thermostability. The difference in the number of hydrogen bonds between pigCS, *Tp*CS, and *Pf*CS is not significant, in contrast to D-glyceraldehyde-3-phosphate dehydrogenase, where a correlation with increasing stability and number of hydrogen bonds was observed (Tanner *et al.*, 1996). No difference exists in the number of helix-capping residues in *Pf*CS or *Tp*CS compared with pigCS, despite the enzymes being entirely α-helical proteins, and neither is there a difference in the number of prolines in β-turns between the three enzymes. Therefore, in citrate synthase at least, these features do not appear to be crucial in conferring hyperthermostability.

Concluding Remarks. The work reported in this paper has permitted the structural comparison of an enzyme across a host temperature range of >60 °C. For this enzyme we observe a trend toward increased compactness of the protein with increasing operating temperature, a significant increase in the number of ion pairs, including a greater number of complex intersubunit ion pair networks, and the elimination of potential "hot spots" for thermal denaturation (e.g., flexible loops and thermolabile residues) by a combination of loop shortening and additional electrostatic interactions.

The crystal structures of seven proteins from organisms that are described as hyperthermophiles (growth temperature >85 °C) have now been reported, and a feature common to all, and most striking in each case, is the large number of ion pairs (intra- and/or intersubunit). This is in contrast to the larger number of crystal structures from thermophilic organisms (growth temperature 55−85 °C) where a "unifying" trend is yet to emerge. Perhaps the ability to withstand relatively moderate temperatures can be achieved by a variety of means, but the very high temperatures under which hyperthermophilic proteins operate represent a structural stress that can only be overcome by a more singular method of interaction.

ACKNOWLEDGMENTS

We thank the staff of EMBL, Hamburg, for their assistance with data collection and the European Union for support of the work at EMBL, Hamburg. We also thank Sue Jones and Janet Thornton (University College, London, U.K.) for performing the gap volume index calculation, and Caroline Lilley and Peter Oliver (University of Bath, Bath, U.K.) for the data on the effects of ligands on thermostability and enzymes kinetics.

REFERENCES

Alter, G. M., Casavva, J. P., Zhi, W., Nemeth, P., Srere, P. A., & Evans, C. A. (1990) *Biochemistry 29*, 7557−7563.
Barlow, D. J., & Thornton, J. M. (1983) *J. Mol. Biol. 168*, 857−885.
Barton, G. J. (1993) *Protein Eng. 6*, 37−40.
Brünger, A. T. (1992) *Nature 355*, 472−475.
Brünger, A. T., Kuriyan, J., & Karplus, M. (1987) *Science 235*, 458−460.
Brünger, A. T., Krukowski, A., & Erickson, J. (1990) *Acta Crystallogr. A46*, 585−593.
CCP4: Collaborative Computational Project No. 4 (1994) *Acta Crystallogr. D50*, 760−763.
Chan, M. K., Mukund, S., Kletzin, A., Adams, M. W. W., & Rees, D. C. (1995) *Science 267*, 1463−1469.
Daggett, V., & Levitt, M. (1993) *J. Mol. Biol. 232*, 600−619.
Daniel, R. M., Dines, M., & Petach, H. H. (1996) *Biochem. J. 317*, 1−11.
Day, M. W., Hsu, B. T., Joshuator, L., Park, J. B., Zhou, Z. H., Adams, M. W. W., & Rees, D. C. (1992) *Protein Sci. 1*, 1494−1507.
DeDecker, B. S., O'Brien, R., Fleming, P. J., Geiger, J. H., Jackson, S. P., & Sigler, P. B. (1996) *J. Mol. Biol. 264*, 1072−1084.
Delboni, L. F., Mande, S. C., Rentier-Delrue, F., Mainfroid, V., Turley, S., Vellieux, F. M. D., Martial, J. A., & Hol, W. G. J. (1995) *Protein Sci. 4*, 2594−2604.
Eriksson, A. E., Baase, W. A., Zhang, X. J., Heinz, D. W., Blaber, M., Baldwin, E. P., & Matthews, B. W. (1992) *Science 255*, 178−183.
Ferrin, T. E., Huang, C. C., Jarvis, L. E., & Langridge, R. (1988) *J. Mol. Graphics 6*, 13−27.
Fersht, A. R., & Serrano, L. (1993) *Curr. Opin. Struct. Biol. 3*, 75−83.
Garman, E. F., & Mitchell, E. P. (1996) *J. Appl. Crystallogr. 29*, 584−587.
Hennig, M., Darimont, B., Sterner, R., Kirschner, K., & Jansonius, J. N. (1995) *Structure 3*, 1295−1306.
Hensel, R. (1993) in *The Archaea* (Kates, M., Kushner, D. J., & Matheson, A. T., Eds.) *New Comprehensive. Biochemistry*, Vol. 26, pp 209−218, Elsevier, Amsterdam, The Netherlands.
Huang, C. C., Petterson, E. F., Klein, T. E., Ferrin, T. E., & Langridge, R. (1991) *J. Mol. Graphics 9*, 230−236.
Jaenicke, R. (1991) *Eur. J. Biochem. 202*, 715−728.
James, K. D., Russell, R. J. M., Parker, L., Daniel, R. M., Hough, D. W., & Danson, M. J. (1994) *FEMS Microbiol. Lett. 119*, 181−186.
Jiang, J.-S., & Brünger, A. T. (1994) *J. Mol. Biol. 243*, 100−115.
Jones, S., & Thornton, J. M. (1995) *Prog. Biophys. Mol. Biol. 63*, 31−69.
Jones, T. A., Zou, J. Y., Cowan, S. W., & Kjeldgaard, M. (1991) *Acta Crystallogr. A47*, 110−119.
Kleywegt, G. J., & Jones, T. A. (1994a) in *From first map to final model: Proceedings of CCP4 study weekend* (Bailey, S., Hubbard, R., & Waller, D., Eds.) pp 59−66, SERC Daresbury Laboratory, Warrington, U.K.
Kleywegt, G. J., & Jones, A. T. (1994b) *Acta Crystallogr. D50*, 178−185.
Knapp, S., Karshikoff, A., Berndt, K. D., Christova, P., Atanasov, B., & Ladenstein, R. (1996) *J. Mol. Biol. 264*, 1132−1144.
Korndörfer, I., Steipe, B., Huber, R., Tomschy, A., & Jaenicke, R. (1995) *J. Mol. Biol. 246*, 511−521.
Kraulis, P. (1991) *J. Appl. Crystallogr. 24*, 946−950.

Kurz, L. C., Shah, S., Frieden, C., Nakra, T., Stein, R. E., Drysdale, G. R., Evans, C. T., & Srere, P. A. (1995) *Biochemistry 34*, 13278−13288.
Luthy, R., Bowie, J. U., & Eisenberg, D. (1992) *Nature 356*, 83−85.
Macedo-Ribeiro, S., Darimont, B., Sterner, R., & Huber, R. (1996) *Structure 4*, 1291−1301.
McDonald, I. K., & Thornton, J. M. (1994) *J. Mol. Biol. 238*, 777−793.
McEvily, A. J., & Harrison, J. M. (1986) *J. Biol. Chem. 261*, 2593−2598.
Menendez-Arias, L., & Argos, P. (1989) *J. Mol. Biol. 206*, 397−406.
Merritt, E. A., & Murphy, M. E. P. (1994) *Acta Crystallogr. D50*, 869−873.
Muir, J. M., Hough, D. W., & Danson, M. J. (1994) *Syst. Appl. Microbiol. 16*, 528−533.
Muir, J. M., Russell, R. J. M., Hough, D. W., & Danson, M. J. (1995) *Protein Eng. 8*, 583−592.
Nakamura, H. (1996) *Q. Rev. Biophys. 29*, 1−90.
Navaza, J. (1992) *Acta Crystallogr. A50*, 157−163.
Nichols, A., Sharp, K. A., & Honig, B. (1991) *Proteins: Struct., Funct., Genet. 11*, 281−296.
Otwinowski, Z., & Minor, W. (1997) *Methods Enzymol. 276*, 307−326.
Perutz, M. F., & Raidt, H. (1975) *Nature 255*, 256−259.
Remington, S. J. (1992) *Curr. Top. Cell. Regul. 33*, 209−229.
Remington, S. J., Wiegand, G., & Huber, R. (1982) *J. Mol. Biol. 158*, 111−152.
Richards, F. M., & Lim, W. A. (1993) *Q. Rev. Biophys. 26*, 423−498.
Richardson, J. S., & Richardson, D. C. (1988) *Science 240*, 1648−1652.
Russell, R. J. M., & Taylor, G. L. (1995) *Curr. Opin. Biotechnol. 6*, 370−374.
Russell, R. J. M., Hough, D. W., Danson, M. J., & Taylor, G. L. (1994) *Structure 2*, 1157−1167.
Sakon, J., Adney, W. S., Himmel, M. E., Thomas, S. R., & Karplus, P. A. (1996) *Biochemistry 35*, 10648−10660.
Shin, D. H., Song, H. K., Seong, I. S., Lee, C. S., Chung, C. H., & Suh, S. W. (1996) *Protein. Sci. 5*, 2236−2247.
Starich, M. R., Sandman, K., Reeve, J. N., & Summers, M. F. (1996) *J. Mol. Biol. 255*, 187−203.
Tanner, J. J., Hecht, R. M., & Krause, K. L. (1996) *Biochemistry 35*, 2597−2609.
Usher, K. C., Remington, S. J., Martin, D. P., & Drueckhammer, D. G. (1994) *Biochemistry 33*, 7753−7759.
Vieille, C., & Zeikus, J. G. (1996) *Trends Biotechnol. 14*, 183−190.
Walker, J. E., Wonacott, A. J., & Harris, J. I. (1980) *Eur. J. Biochem. 108*, 581−586.
Wallace, A. C., Laskowski, R. A., & Thornton, J. M. (1995) *Protein. Eng. 8*, 127−134.
Watanabe, K., Masuda, T., Ohashi, H., Mihara, H., & Suzuki, Y. (1994) *Eur. J. Biochem. 226*, 277−283.
Woese, C. R., Kandler, O., & Wheelis, M. L. (1990) *Proc. Natl. Acad. Sci. U.S.A. 87*, 4576−4579.
Yip, K. S. P., Stillman, T. J., Britton, K. L., Artymuik, P. J., Baker, P. J., Sedelnikova, S. E., Engel, P. C., Pasquo, A., Chiaraluce, R., Consalvi, V., Scandurra, R., & Rice, D. W. (1995) *Structure 3*, 1147−1158.

BI9705321